Thermal Fluctuations in Superconductor/Ferromagnet Nanostripes

Introduction

The problem of fluctuations in two-dimensional (2-D) superconducting stripes with a thickness d that is much smaller than the London penetration depth λ and a width w that is much smaller than the Pearl length $\Lambda = 2\lambda^2/d \gg w$ has been extensively discussed in the context of the Berezinsky–Kosterlitz–Thouless (BKT) transition.[1,2] The interest in this topic was revived recently[3,4] to try to better understand the physics of the operation of superconducting single-photon detectors (SSPD's) consisting of nanostripes that are densely packed into a meander-type geometry. The first SSPD's introduced in 2001 (Ref. 5) have since received great attention because of their excellent performance as ultrafast, highly efficient counters for both infrared and visible light photons and are now regarded as the devices of choice in such high-performance applications such as quantum optics and quantum communications.[6,7] The SSPD basic model of operation principle is based on a supercurrent-to-resistive-state transition of a 2-D nanostripe maintained at a temperature far below the critical temperature T_c and biased sufficiently close to its critical current I_c. The energy of one or several optical photons absorbed in the nanostripe is sufficient to trigger the transition, producing a transient resistive state and resulting in a detection event.

Independent of the photon counts described above and even when completely isolated from any external light, the SSPD spontaneously generates (especially at higher operating temperatures and with the bias close to I_c) transient voltage pulses. Fully understanding the nature of dark counts, i.e., the physical mechanism of these fluctuation events, is very relevant for optimizing the counting performance of SSPD's (minimization of their dark counts). In addition, the dark-count phenomenon has its own basic physics interest in relation to dissipation and thermal fluctuation effects occurring in superconducting 2-D nanostripes and 1-D (one-dimensional) nanowires.

The present literature on dark counts in SSPD's focuses exclusively on NbN-based devices[3,4,8,9] and most recently favors the explanation that assigns the most-relevant role to magnetic vortices moving across the width of a superconducting stripe, either as vortex–antivortex pairs (VAP's) or as single vortices overcoming the barrier at opposite edges of the stripe—a mechanism called vortex hopping (VH). In other proposals, relevant mechanisms consider thermal fluctuations of the number of excitations[8] or spontaneous nucleation of normal-state regions across the stripe in analogy with 2π-phase slip centers existing in 1-D wires,[10,11] but the latter process is typically discarded because its occurrence has a low probability in 2-D superconducting nanostripes, typically implemented in practical SSPD's.

Besides NbN, a number of superconducting materials have been proposed and successfully implemented for SSPD applications: for example, WSi and MoSi[12,13] or hybrid superconductor/ferromagnet (S/F) bilayers.[14] Therefore, it is important to note that the composition and morphology of different materials may lead to significant variations in fluctuation mechanisms. In this respect, the investigation of S/F bilayers is of particular interest because, as we have already demonstrated elsewhere,[14–16] the presence of a weak ferromagnetic overlayer significantly influences both the superconducting and optical properties of the S/F nanostripes. In fully proximitized, hybrid S/F nanostructures, such as NbN/NiCu, vortex pinning effects are certainly of relevance, leading, e.g., to the J_c enhancement.[14] At the same time, even an epitaxial-quality S/F interface leads to a significant change in the electron nonequilibrium relaxation dynamics observed in photoresponse experiments.[15,16] Consequently, the S/F systems constitute a great test bed for investigating the role of magnetic vortices in fluctuation phenomena in 2-D superconducting nanostripes and can provide a direct comparison between various models that have been proposed in the literature. The latter is greatly facilitated by the fact that all test structures, as well as the pure-S reference samples, can be processed in the same fabrication run and tested under exactly the same conditions. Finally, besides their unquestionable role in dark counts, vortices have also been implicated as a possible reason for the appearance of photon counts in SSPD's, at least as a supplementary detection mechanism.[17,18] They are, in fact, likely to play a key role in the nonequilibrium photoresponse mechanism of high-temperature superconducting photodetectors.[19]

In this work, the effects of thermal fluctuations in super-conducting hybrid S/F nanostructures are investigated and compared with those observed in pure-S nanostripes. The hybrid S/F samples are 5-μm-long, 175-nm-wide nanostripes that consist of an 8-nm-thick NbN film covered with a 6-nm-thick NiCu, weak ferromagnet overlayer, while the reference samples are 5-μm-long, 100-nm-wide, 8-nm-thick NbN, pure-S nanostripes. The experimental dependences of the fluctuation rates as functions of bias current and temperature are presented and discussed in the framework of both the VAP and VH theoretical models. Arguments are provided for why other possible fluctuation mechanisms are excluded and, instead, focused only on the VAP and VH scenarios. Most importantly, the studies, as suggested by Bartlof *et al.*,[3] made it possible to differentiate between the VAP and VH models.

The following sections will (1) describe the sample fabrication and characterization and present time-resolved dark- and photon-count waveforms and measurements of the thermal fluctuation rates versus the bias current and temperature; (2) outline the main features of both the VAP and VH theoretical models, which were then used to interpret the experimental data; and (3) present conclusions and future outlook.

Experimental Details and Results

The base of superconducting nanostripes tested in this work was 8-nm-thick NbN film grown on MgO substrates by reactive dc-magnetron sputtering in an Ar/N_2 gas mixture under general sputtering conditions reported elsewhere.[14–16] For S/F structures, a NiCu overlayer was deposited in the same system, without breaking vacuum, by a dc magnetron in pure Ar equipped with a $Ni_{0.39}Cu_{0.61}$ target at a 155-W deposition power and a rate of 60 nm/min, respectively. Magnetic moment tests demonstrated that our NiCu overlayers were ferromagnetic with a Curie temperature of ~20 K. All tested nanostripes were patterned by electron-beam lithography, followed by reactive-ion etching. Gold contacts were defined by conventional photolithography and the lift-off method. For thermal fluctuation measurements, 5-μm-long straight nanostripes were used with a width of 175 nm and 100 nm for NbN/NiCu and NbN, respectively. The NbN stripes exhibited $T_c = 12.1\pm0.2$ K, while the T_c values of the NbN/NiCu samples were suppressed by less than 0.5 K.

From current–voltage (I–V) characteristic measurements of the nanostripes, performed at different temperatures, critical-current-density dependences were obtained for $J_c^{NbN/NiCu}(T)$ and $J_c^{NbN}(T)$, for NbN/NiCu and NbN nanostripes, respectively. In agreement with the authors' previously published
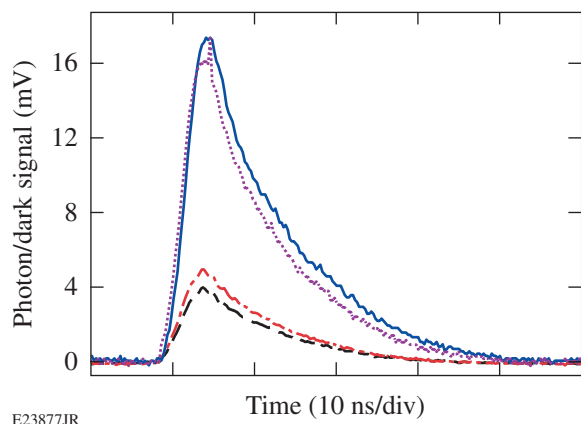
experiments,[14] J_c's for NbN/NiCu nanostructures were significantly enhanced as compared to those of NbN and, for example, at 4.2 K, $J_c^{NbN/NiCu} = 43.2$ MA/cm^2, while $J_c^{NbN} = 11.6$ MA/cm^2. The J_c enhancement in the S/F bilayer was explained in Ref. 14 as the impact of scalar magnetic impurities[20] that generate extra flux pinning in fully proximitized S/F film.

To measure the dark-count rate, the samples were mounted on a cryogenic insert and placed them inside a liquid-helium transport Dewar. The sample holder was surrounded by a metallic enclosure that completely shielded the test structure from outside radiation. The sample temperature was controlled by varying the helium vapor pressure and position of the insert inside the Dewar and was measured with a calibrated germanium thermometer. The dark-count events were registered as voltage-fluctuation transients and readout using a cascade of two microwave amplifiers with an effective bandwidth of 0.1 to 100 MHz and a total gain of 20 dB. The amplified signals were fed by a 50-Ω coaxial cable into readout electronics, which consisted of either a digital oscilloscope with a 1-GHz bandwidth or a pulse counter with a 100-MHz bandwidth.

As a reference, the measured photon counts were obtained by illuminating the same nanostripes with 6.25-ns-wide, 1550-nm-wavelength laser pulses, generated by a laser diode with a repetition rate of 80 MHz. The laser-spot diameter was ~50 μm, much larger than the size of the nanostripe, ensuring a uniform optical illumination. The latter tests were done in a continuous-flow helium cryostat with an optical window.

Figure 142.18 presents examples of time-resolved waveforms of dark and photon counts, measured at $T = 4.9$ K, for both NbN/NiCu and NbN nanostripes biased at the same value of a normalized bias current, namely $I_b/I_c = 0.8$. Note that for each nanostripe, the dark- and photon-count pulses practically overlap since in both cases the transient voltage signals reflect the resistive state of a nanostripe. Actually, all four waveforms in Fig. 142.18 have the identical shape with a detection-system–limited rise time and an ~20-ns-long fall time. The difference in the amplitude between the NbN/NiCu and NbN signals (the S/F sample exhibits a significantly larger amplitude) is a result of the earlier-mentioned difference in their respective J_c's; in fact, the amplitude ratio is very close to the $J_c^{NbN/NiCu}\big/J_c^{NbN}$ ratio.

Figure 142.19 presents thermal fluctuation or dark-count rates of NbN (black squares) and NbN/NiCu (red circles) nanostripes as functions of I_b/I_c at temperatures 4.5, 6.0, and 8.0 K, collected using a pulse counter. For both nanostripes, the fluctuation

Figure 142.18
Photon- and dark-count pulses of NbN (red and black lines, respectively) and NbN/NiCu (magenta and blue lines, respectively) nanostripes. All pulses were recorded under the same conditions, namely, $I_b/I_c = 0.8$ and $T = 4.9$ K. For photon illumination, we used pulsed laser illumination with a 1550-nm wavelength.

difference is that the former dataset was fitted (solid lines) using the VAP model, while the latter dataset was fitted using the VH model. The details of the fits and their physical significance are presented in the next section.

Fluctuation Models and Discussion

In 2-D systems, both transverse dimensions (d and w) of a superconducting stripe should be smaller than the shortest relevant scale, which in this case is given by the Ginzburg–Landau coherence length ξ. Literature[3,9] values of ξ_0, the coherence length at $T = 0$, for NbN are of the order of a few nanometers, and from superconducting fluctuation measurements,[21] it is expected that ξ_0 for NbN/NiCu should be even slightly shorter. Therefore, it can be assumed that the nanostripes fall into the 2-D category. Moreover, the Likharev condition $w \geq 4.4\xi$ is always satisfied, ensuring that the stripes are wide enough to nucleate their propagation of vortices. Finally, $\Lambda \gg w$; therefore, the current-density distribution can be assumed to be homogeneous across the film widths.
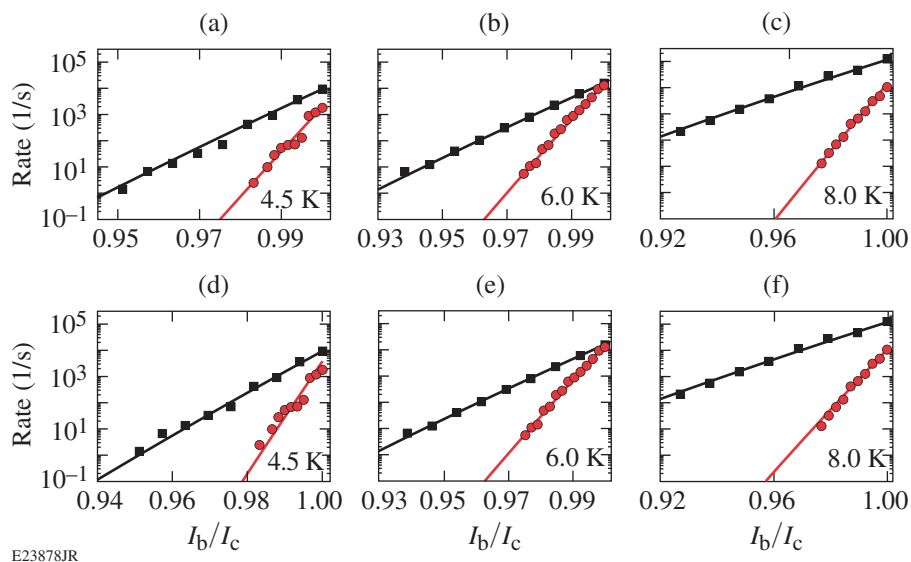
rates were observed to decrease exponentially over four orders of magnitude. The S/F sample is, however, much more stable against fluctuations, exhibiting significantly lower dark counts at each temperature. In all panels in Fig. 142.19, the I_b/I_c range of the measurements was limited by the 1-Hz accuracy of the counter. Finally, it is stressed that the experimental data (black squares and red circles) presented in Figs. 142.19(a)–142.19(c) are exactly the same as those in Figs. 142.19(d)–142.19(f). The

Various mechanisms are able to produce dark counts and could be considered as responsible for the fluctuation rates measured in these experiments. They can be summarized as (1) thermal unbinding of VAP's; (2) thermal or quantum mechanism of VH; (3) fluctuations of the number of quasiparticles; and (4) thermal or quantum phase-slip center processes. Following the arguments given in Ref. 3, based on a comparison

Figure 142.19
Measured fluctuation rates versus normalized bias current of NbN (black squares) and NbN/NiCu (red circles) nanostripes, measured at 4.5, 6.0, and 8.0 K. The solid lines are the best fits obtained using the [(a)–(c)] VAP model and the [(d)–(f)] VH model.

of the amplitudes of the excitation energy barriers, it can be concluded that the probability of an occurrence of phase-slip centers is very low, so it can be ignored in this process. Next, following a theoretical approach presented in Ref. 8, the dark-count rate related to the fluctuation in the number of quasi-particles is calculated, but any attempt to fit the data with this model failed, in particular for the S/F sample. Finally, since the temperature interval investigated in this work is 4.5 to 8.0 K, fluctuation mechanisms caused by quantum tunneling of vortices through the edge barrier can be excluded because they become relevant only at sub-Kelvin temperatures.[11]

Based on the above, discussion is limited to the thermal regime and consider only the VAP and VH fluctuation scenarios:

(1) VAP: unbinding of vortex–antivortex pairs and their movement across the nanostripe to its opposite edges resulting from the Lorentz force;

(2) VH: thermal excitation of a single vortex near the edge of the stripe and a consecutive dissipative movement across it.

In both models, thermal fluctuations must overcome an excitation energy barrier $U(I_b,T)$ and the corresponding fluctuation, or, equivalently, the dark-count rate may be expressed as

$$\Gamma(I_b,T) = \Omega \exp\left[-U(I_b,T)/k_B T\right], \qquad (1)$$

where Ω is the attempt frequency. The actual expressions for $U(I_b,T)$, as well as the fit values of Ω, will, of course, be different in these two types of mechanisms.

1. Unbinding of Vortex–Antivortex Pairs

In 2-D systems, the collapse of a long-range order gives rise to so-called topological defects in the order parameter that, in thin superconducting films, excite pairs of vortices, according to the BKT model. At temperatures below the BKT transition, these pairs consist of single vortices with their respective supercurrents circulating in opposite directions and result in a bound VAP state. Under the $w \geq 4.4\xi$ condition, a BKT phase transition can occur only if the energy of a bound VAP depends logarithmically on the separation distance of the vortex core centers $r(r \ll \Lambda)$. Under a transport current condition, however, a Lorentz force is exerted on VAP's and directed in opposite directions for the vortex and the antivortex, respectively. The resulting torque forces VAP's to align perpendicularly to the current flow. The binding energy changes with the angle and reaches its minimum at $\pi/2$. As was shown by Mooji,[22] the interplay between repulsion of vortices in a pair resulting

from the Lorentz force and their magnetic attraction defines the current-dependent $r = 2.6\xi I_c/I_b$, leading to the minimal binding energy of the pair, U_{VAP} (Ref. 3).

This binding energy may be overcome by thermal excitations with a probability equal to the Boltzmann's factor $\exp(-U_{VAP}/k_B T)$. In the absence of pinning, thermally unbound vortices will move freely toward opposite edges of the strip, where they leave the structure or rather annihilate with an oppositely oriented vortex. The moving vortices dissipate energy, initiating creation of a nonsuperconducting domain. In current-biased $(I_b < I_c)$ stripes, the appearance of such domains results in voltage transients that are then registered as dark-count events. According to the model in Refs. 3 and 8, the dark-count rate follows Eq. (1) with the U_{VAP} given by

$$U_{VAP} = \frac{A(T)}{\varepsilon}\left[\ln\left(\frac{2.6I_c}{I_b}\right) - 1 + \frac{I_b}{2.6I_c(T)}\right], \qquad (2)$$

where $A(T)$ is the vortex interaction constant and ε is the averaged polarizability of a VAP within the entire VAP population.[3,22]

The solid lines in Figs. 142.19(a)–142.19(c) present the fits of the fluctuation rates for both NbN and NbN/NiCu samples based on Eqs. (1) and (2) at three different temperatures. The values of the fitting parameters, $A(T)$ and ε, are reported in Table 142.IV (Ref. 23). We note that the fits are in agreement with the experimental data and the $A(T)$ and ε values are reasonably close to those reported in the literature.[3] Interestingly, the A parameter for the NbN/NiCu sample has a value about three times greater than that for the NbN sample, indicating that the binding energy of the VAP in this case is significantly stronger than in the pure NbN. The latter explains the dramatically lower (over an order of magnitude) fluctuation rates for the NbN/NiCu nanostripe, as compared to NbN. The presence of a weak ferromagnetic NiCu layer also leads to an increase of ε, providing clear evidence that pinning is enhanced in the S/F sample.

2. Vortices Overcoming the Edge Barrier

The experimental data is analyzed in a framework of the motion of single unbounded vortices.[3,4] At bias currents close to the de-pairing I_c, the magnetic self-field at the stripe edges is much larger than the critical field for vortex entry. The entry of vortices at one edge of the stripe and antivortices at the opposite edge is prohibited by an edge barrier very similar to the Bean–Livingston surface barrier.[3,24] Consequently, the corresponding probability for thermally activated vortex hopping

Table 142.IV: Parameters used to fit the measured fluctuation rates within the VAP and VH models.

Samples	T (K)	VAP model fitting parameters		VH model fitting parameters		Calculated parameters	
		A (eV)	ε	ξ (nm)	E_B (eV)	Λ (μm)	λ (nm)
NbN	4.5	0.20	1.9	4.5	0.10	34	368
	6.0	0.19	1.8	5.9	0.09	37	385
	8.0	0.16	1.8	6.9	0.08	44	420
NbN/NiCu	4.5	0.70	3.0	4.3	0.35	9.7	261
	6.0	0.66	2.5	5.0	0.34	10.3	269
	8.0	0.65	2.0	6.0	0.33	10.4	270

over this energy barrier is again proportional to the Boltzmann factor $\exp\left(-U_{VH}/k_B T\right)$. However, U_{VH} is now given by

$$U_{VH}(T, I_b) = E_B(T, I_b)$$

$$\times\left(\ln\left\{\frac{2w}{\pi\xi(T)}\frac{1}{\sqrt{1+\left[\Phi_0 I_b/\pi E_B(T, I_b)\right]}}\right\}\right.$$

$$\left.-\frac{\Phi_0 I_b}{\pi E_B(T, I_b)}\left\{\arctan\left[\frac{\pi E_B(T, I_b)}{\Phi_0 I_b}\right]-\frac{\pi\xi(T)}{2w}\right\}\right), \quad (3)$$

where $E_B(I_b, T) = \Phi_0^2/2\pi\mu_0\Lambda(I_b, T)$ is the energy scale.[3]

Once a vortex jumps over the barrier, thanks to the Lorentz force, it will move across the stripe. Analogically to the VAP scenario, motion of these free vortices across the stripe creates a nonsuperconducting domain and results in a voltage transient. The resulting dark-count rate for the VH process is given by Eq. (1) with U_{VH} defined in Eq. (3).

In Figs. 142.19(d)–142.19(f), the solid lines are the fits of the experimental fluctuation rates (circles) for the NbN and NbN/NiCu samples, but this time using Eqs. (1) and (3). Note that beside the NbN/NiCu data at 4.5 K, the fits are as good as in the case of the VAP model. The E_B and ξ fitting parameters are reported in Table 142.IV (Ref. 23) next to the column representing the VAP model. First of all, a clear self-consistency of the thermal fluctuation approach is noticed, i.e., $E_B = A/2$, as expected from the definition of E_B. The extracted value of E_B made it possible to calculate the parameter Λ and, consequently, λ for the samples at the three temperatures studied. The actual values are listed in a separate column in Table 142.IV; for NbN/NiCu, both Λ and λ are somewhat reduced as compared to NbN.

The $\xi(T)$ values obtained with the fitting procedure of the VH model for both NbN and NbN/NiCu nanostripes are plotted in Figs. 142.20(a) and 142.20(b), respectively, as a function of normalized temperature T/T_c. As expected earlier, the presence of the NiCu overlayer enhances the S/F nanostripe 2-D character by reducing the $\xi(T)$ values, as compared to the pure NbN sample. The solid lines are the best fits of these values obtained by using the following analytical expression [Eq. (3)]:

$$\xi^2(T/T_c) = \frac{\xi_0^2}{\left(1-T/T_c\right)}\frac{1}{\sqrt{1+T/T_c}}. \quad (4)$$

The $\xi(T)$ values extracted from the fits carry rather large errors (especially at higher temperatures), but the agreement with Eq. (4) is still very good and makes it possible to estimate the ξ_0 values as equal to 3.9 nm and 4.2 nm for the NbN/
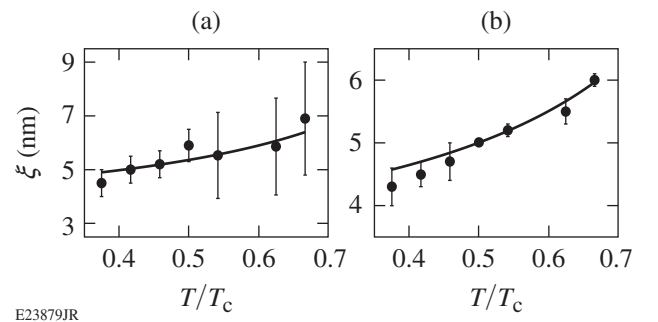

Figure 142.20
The coherence length's dependence on the normalized temperature for (a) NbN and (b) NbN/NiCu samples. The $\xi(T)$ values (circles) were obtained by the best-fitting procedure [Eqs. (1) and (3)] to the VH model (see also Fig. 142.19). The solid lines are the best fits obtained by using Eq. (4). The extrapolated values of ξ_0 are 4.2 nm and 3.9 nm for NbN and NbN/NiCu samples, respectively.

NiCu and NbN samples, respectively. The obtained ξ_0 values reinforce the fact that the 2-D approximation is applicable for our nanostripes.

3. Discussion

A simple "visual" comparison between Figs. 142.19(a)–142.19(c) and 142.19(d)–142.19(f) does not enable the differentiation between which of the two vortex-based, thermal fluctuation scenarios best describes the physics of our experiments. Therefore, we have attempted a more-quantitative approach by plotting the values of the excitation energy in units of k_B at the fixed $I_b/I_c = 0.99$ bias as functions of temperature. The results are plotted in Fig. 142.21. The points correspond to the U_{VAP}/k_B and U_{VH}/k_B values for both the NbN and NbN/NiCu samples (see Fig. 142.21 caption for details), and the solid lines are only guides for the eye.
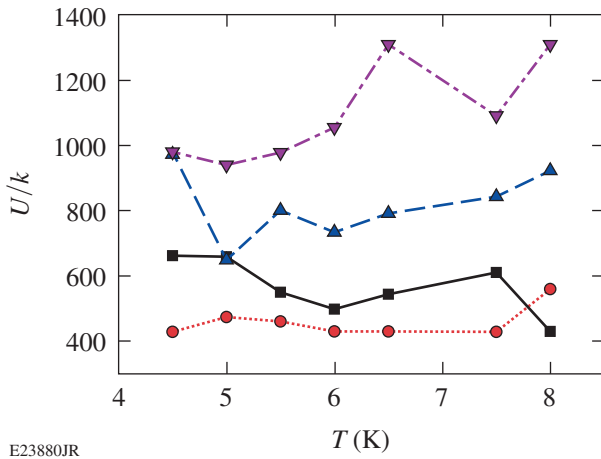

E23880JR

Figure 142.21
Excitation energy U in units of k_B at seven temperatures. The plotted points are the best-fit values from Fig. 142.19 at $I_b/I_c = 0.99$; the corresponding symbols are magenta inverted triangles: VAP, NbN/NiCu; blue triangles: VH, NbN/NiCu; red circles: VAP, NbN; and black squares: VH, NbN. The lines are only guides for the eye.

Individual comparisons between the data corresponding to S/F and S samples within the same fluctuation model are made, as well as comparisons between the VAP and VH models for the same sample type. Within the VAP model, the data for NbN (red circles) and NbN/NiCu (magenta inverted triangles) show that the excitation energy of the pure NbN sample is always significantly smaller than that of the NbN/NiCu sample, i.e., $U_{VAP}^S < U_{VAP}^{S/F}$. In addition, the same behavior (although not as dramatic) is also observed within the VH model for NbN (black squares) and NbN/NiCu (blue triangles) samples. The latter is a clear confirmation that the stronger pinning existing in the

S/F nanobilayer corresponds to the higher-energy excitation barrier and, as a consequence, leads to a significant decrease in the rate of thermal fluctuations (dark counts) observed in Fig. 142.19 for the NbN/NiCu nanostripe.

Next, the two models are compared for the same sample type, i.e., NbN/NiCu (blue triangles) with NbN/NiCu (magenta inverted triangles) and NbN (black squares) with NbN (red circles). From Fig. 142.21 it is noted that for the S/F sample, the excitation energy corresponding to the VH model (blue triangles) is always markedly lower than that of the VAP model (magenta inverted triangles), i.e., $U_{VH}^S < U_{VAP}^{S/F}$. The only exception is the $T = 4.5$-K data point, but as previously mentioned, the VH fit in this case is uncharacteristically poor [see Fig. 142.19(d)], and can be disregarded at this point. Consequently, the presence of extra pinning in the S/F sample makes it possible to differentiate between the two mechanisms, and the VH scenario with the lower U_{VH} barrier is clearly favored for S/F samples. On the other hand, for the pure-S sample, the VH and VAP values are quite close and differentiation is difficult. However, Fig. 142.21 seems to indicate that the VAP mechanism is favored in the NbN sample, supporting earlier findings.[9]

Conclusions

The fluctuation rate as a function of the applied bias current was measured at various temperatures in hybrid S/F and pure-S nanostripes and have performed the same NbN/NiCu and NbN sample measurements of the I–V characteristics and the time-resolved waveforms of both photon- and dark-count events. The NbN/NiCu samples exhibited an enhancement of I_c; correspondingly, the amplitude increase of both the photon- and dark-count pulses were measured. The latter findings clearly indicate the role of pinning of magnetic vortices in S/F nanostructures and confirm the results obtained previously on similar samples.[14] The measured fluctuation rates have been analyzed in a framework of the VAP and VH theoretical models that are based on thermal activation and subsequent motion of magnetic vortices. In the fluctuation rate versus temperature experiments, the NbN/NiCu samples were significantly more stable against thermal fluctuation as compared to NbN, and for NbN/NiCu a mechanism based on thermal VH was clearly dominant. The model discrimination was less evident in the case of pure-S samples; nevertheless, the results point to the VAP mechanism as being responsible for the dark counts observed in NbN nanostripes, in agreement with earlier studies.[9]

For the practical application of nanostripes as SSPD's, the detailed knowledge of the physical origin of thermal

fluctuations is important to improving the performance of superconducting detectors by controlling their dark counts. Hybridization of a pure superconducting nanostripe with a weak ferromagnetic material, as in the case of the NbN/NiCu sample, is very promising since it leads to a significant decrease in thermal fluctuations that corresponds to reduced dark counts, as well as in the increase in the photoresponse amplitude, resulting in an improved signal-to-noise ratio of the SSPD.

ACKNOWLEDGMENT

REFERENCES

1. Y. Liu *et al.*, Phys. Rev. Lett. **68**, 2224 (1992).

2. J. M. Repaci *et al.*, Phys. Rev. B **54**, R9674 (1996).

3. H. Bartolf *et al.*, Phys. Rev. B **81**, 024502 (2010).

4. L. N. Bulaevskii *et al.*, Phys. Rev. B **83**, 144526 (2011).

5. G. N. Gol'tsman, O. Okunev, G. Chulkova, A. Lipatov, A. Semenov, K. Smirnov, B. Voronov, A. Dzardanov, C. Williams, and R. Sobolewski, Appl. Phys. Lett. **79**, 705 (2001).

6. R. H. Hadfield, Nat. Photonics **3**, 696 (2009).

7. C. M. Natarajan, M. G. Tanner, and R. H. Hadfield, Supercond. Sci. Technol. **25**, 063001 (2012).

8. A. Engel *et al.*, Physica C **444**, 12 (2006).

9. J. Kitaygorsky, I. Komissarov, A. Jukna, D. Pan, O. Minaeva, N. Kaurova, A. Divochiy, A. Korneev, M. Tarkhov, B. Voronov, I. Milostnaya, G. Gol'tsman, and R. Sobolewski, IEEE Trans. Appl. Supercond. **17**, 275 (2007).

10. J. S. Langer and V. Ambegaokar, Phys. Rev. **164**, 498 (1967).

11. D. S. Golubev and A. D. Zaikin, Phys. Rev. B **64**, 014504 (2001).

12. F. Marsili *et al.*, Nature Photon. **7**, 210 (2013).

13. Yu. P. Korneeva *et al.*, Supercond. Sci. Technol. **27**, 095012 (2014).

14. N. Marrocco *et al.*, Appl. Phys. Lett. **97**, 092504 (2010).

15. D. Pan, G. P. Pepe, V. Pagliarulo, C. De Lisio, L. Parlato, M. Khafizov, I. Komissarov, and R. Sobolewski, Phys. Rev. B **78**, 174503 (2008).

16. T. Taneda, G. P. Pepe, L. Parlato, A. A. Golubov, and R. Sobolewski, Phys. Rev. B **75**, 174507 (2007).

17. J. J. Renema *et al.*, Phys. Rev. B **87**, 174526 (2013).

18. J. J. Renema *et al.*, Phys. Rev. Lett. **112**, 117604 (2014).

19. R. Arpaia, M. Ejrnaes, L. Parlato, F. Tafuri, R. Cristiano, D. Golubev, R. Sobolewski, T. Bauch, F. Lombardi, and G. P. Pepe, Physica C **509**, 16 (2015).

20. A. I. Buzdin, Rev. Mod. Phys. **77**, 935 (2005).

21. W. Lang, University of Vienna, private communication (2015).

22. J. E. Mooij, in *Percolation, Localization, and Superconductivity*, edited by A. M. Goldman and S. A. Wolf, NATO ASI, Series B, Vol. 109 (Plenum Press, New York, 1984), pp. 325–370.

23. The attempt frequency Ω is the third fitting parameter in both models. Our fitted values are close to that of Ref. 3. They are not shown in Table 142.IV because of their irrelevance to the discussion.

24. C. P. Bean and J. D. Livingston, Phys. Rev. Lett. **12**, 14 (1964).